Supporting Information

Ionically Engineered $Zn@Fe_3O_4$ Nanocomposite Hydrogels with Stretchable Mechanics and High-Performance Electrochemical Storage for Wearable Supercapacitors and Strain Sensors

Azaz Ali Khan[1], Ibrar Ahmad[1], Daixin Ye[2], Luqman Ali Shah[1,2]*

[1]*Polymer Laboratory, National Centre of Excellence in Physical Chemistry, University of Peshawar, Peshawar 25120 Pakistan*

[2]*Institute for Sustainable Energy, College for Sciences, Shanghai University, Shanghai, 200444, China*

*Corresponding author

Email: luqman_alisha@uop.edu.pk

Tel: (9291)9216766

S1. Experimental Section

S1.1 Materials for Composite NPs

Chemical co-precipitation technique was used to synthesize composite Zn-doped-magnetite NPs ($Zn@Fe_3O_4$). In this work, ≥99.0% (RT), puriss. p.a. Ferrous Chloride tetrahydrate ($FeCl_2{\cdot}4H_2O$, 13478-10-9), ACS reagent, crystallized, 98.0-102% (RT) Ferric Chloride hexahydrate ($FeCl_3{\cdot}6H_2O$, 10025-77-1), DEAJUNG reagent, 98% Zinc nitrate hexahydrate ($Zn(NO_3)_2{\cdot}6H_2O$, 10196-18-6), 97-100.5% Sodium hydroxide (NaOH, 1310-73-2), ≥99.8%, ACS reagent, ethyl alcohol (C_2H_6O, 64-17-5), and Milli-Q double deionized water was used. All the reagents were of analytical grade and used without any further treatment.

S1.2 Synthesis of Zn-doped Fe_3O_4 NPs

Supporting Information

Zn-doped magnetite ($Zn_xFe_{3-x}O_4$, where $x \approx 0.1$) nanoparticles (NPs) were synthesized via a chemical co-precipitation method. Initially, stoichiometric amounts of ferric chloride hexahydrate ($FeCl_3 \cdot 6H_2O$, 2.22 g) and ferrous chloride tetrahydrate ($FeCl_2 \cdot 4H_2O$, 0.77 g) were dissolved in distilled water, maintaining a Fe^{3+} to Fe^{2+} molar ratio of 2:0.9. The solution was stirred vigorously at 80 °C for 2 hours. To achieve approximately 3.5 mol% Zn doping (targeting $x \approx 0.1$ in $Zn_xFe_{3-x}O_4$), an aqueous solution of a zinc salt was added dropwise to the iron precursor under continuous stirring to ensure uniform distribution of Zn^{2+} ions. Subsequently, a 2.0 M NaOH solution was slowly introduced until the pH reached ~13, promoting the co-precipitation of the Zn-doped Fe_3O_4 NPs. The resulting black precipitate was separated using a magnet, centrifuged at 9000 rpm for 30 minutes, and washed repeatedly with distilled water and ethanol until the pH decreased to ~6.5. Finally, the product was dried in a vacuum oven at 400 °C for 4 hours and ground into fine nano-powder[1].

S2. Results and Discussion

S2.1 Characterization of pure $Zn_xFe_{3-x}O_4$ NPs

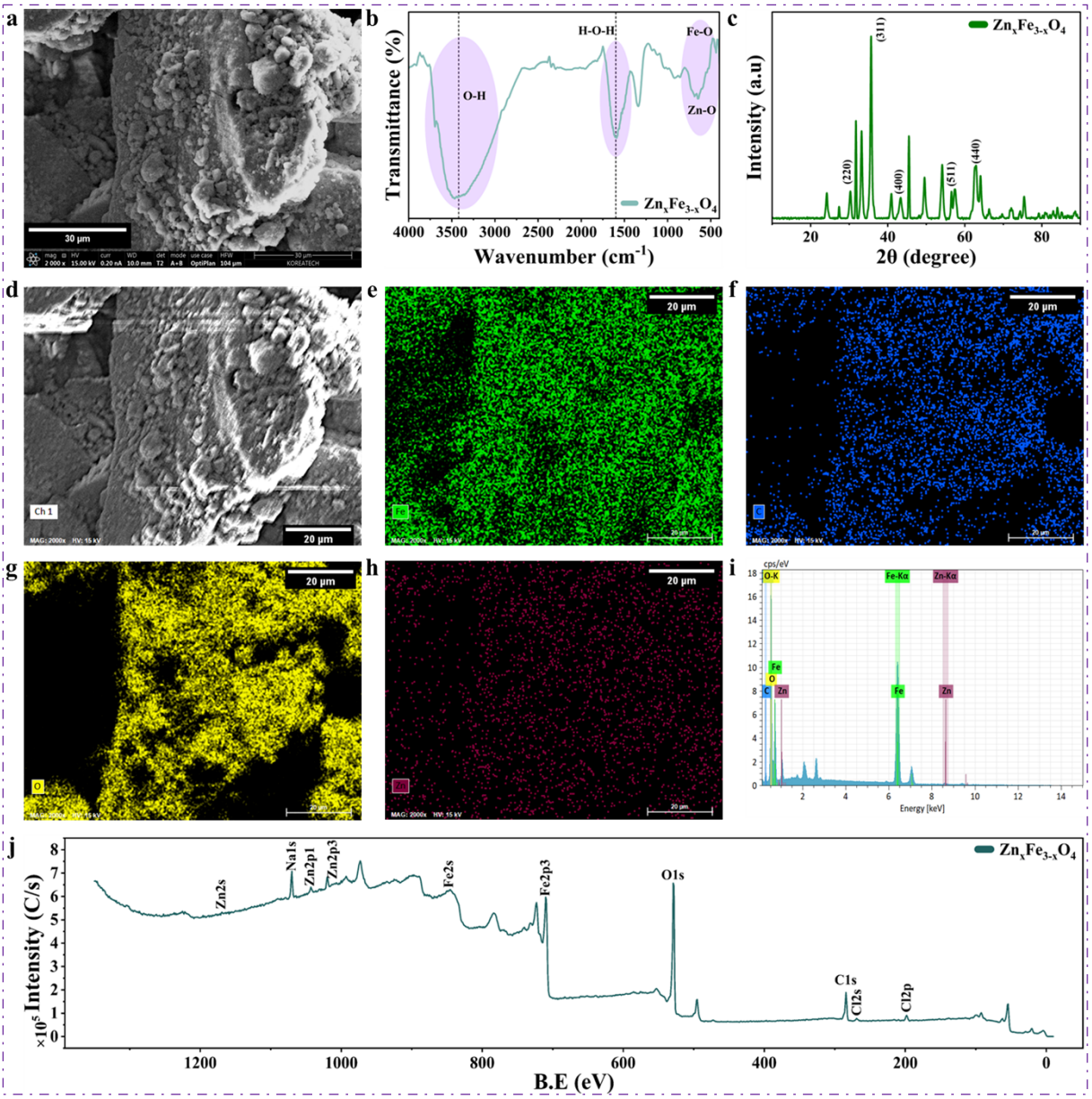

Figure S1. (a) SEM image showing the morphology of Zn-doped Fe_3O_4 nanoparticles (NPs) at a scale of 30 µm. **(b)** FTIR spectrum of Zn-doped Fe_3O_4 NPs highlighting the characteristic functional groups. **(c)** XRD pattern confirming the crystalline structure of Zn-doped Fe_3O_4 NPs. **(d–i)** EDS elemental analysis illustrating the composition and confirming the presence of Zn, Fe, and O in the NPs. **(j)** High-resolution XPS spectra of $Zn_xFe_{3-x}O_4$ NPs showing the characteristic peaks of Fe, Zn, and O, confirming their incorporation within the spinel oxide structure.

Supporting Information

The surface morphology of the $Zn_xFe_{3-x}O_4$ nanoparticles (NPs) was characterized using field emission scanning electron microscopy (FE-SEM), as presented in Figure S1a. The images show that the NPs possess a generally spherical shape with noticeable agglomeration an expected behavior for spinel ferrite NPs, primarily due to their magnetic interactions and elevated surface energy. The average particle size was estimated to range between 30 and 60 nm, indicating effective nano-structuring achieved through the employed synthesis approach. FTIR spectroscopy was also performed on the synthesized $Zn_xFe_{3-x}O_4$ NPs to verify the formation of the spinel structure. As illustrated in Figure S1b, a broad absorption band around 3420 cm^{-1} corresponds to O–H stretching vibrations from surface hydroxyl groups and adsorbed moisture, while a prominent peak at approximately 1600 cm^{-1} is attributed to H–O–H bending of physically adsorbed water. The most distinctive signals appear in the 600–400 cm^{-1} region, where absorption bands near 580 cm^{-1} and 470 cm^{-1} are associated with Fe–O and Zn–O stretching vibrations in the tetrahedral and octahedral sites of the spinel lattice. These features align closely with reported values for $Zn_xFe_{3-x}O_4$, confirming the successful formation of the ferrite phase. The close correspondence with reference spectra further validates the phase purity and structural fidelity of the synthesized NPs[1]. The crystalline structure of the synthesized $Zn_xFe_{3-x}O_4$ NPs was confirmed by X-ray diffraction (XRD) analysis, as shown in Figure S1c. The diffraction pattern exhibited distinct peaks at 2θ values of approximately 30.1°, 35.4°, 43.1°, 56.9°, and 62.5°, which correspond to the (220), (311), (400), (511), and (440) planes of the spinel $Zn_xFe_{3-x}O_4$ structure, respectively. These peaks are in good agreement with the standard Joint Committee on Powder Diffraction Standards (JCPDS) card No. 22-1012, confirming the formation of a well-defined spinel phase[1]. The absence of impurity peaks further indicates the high purity and phase integrity of the synthesized NPs[2]. The elemental composition of $Zn_xFe_{3-x}O_4$ NPs was confirmed by energy-dispersive X-ray spectroscopy (EDS), as shown in Figure S2(d–i). The EDS spectrum exhibits distinct peaks corresponding

to Zn, Fe, and O, with no detectable impurities, confirming the successful and high-purity synthesis of $Zn_xFe_{3-x}O_4$. Moreover, the elemental ratios are in close agreement with the expected stoichiometry of Zn:Fe:O for the spinel $Zn_xFe_{3-x}O_4$ structure. The corresponding elemental compositions are summarized in Table S1. The X-ray photoelectron survey spectrum of $Zn_xFe_{3-x}O_4$ NPs displays the characteristic signals of Fe, Zn, and O, confirming their presence in the oxide framework. A weak carbon contribution is also detected, which can be attributed to minor surface contamination from air exposure. The elemental composition obtained from the survey indicates that Zn is successfully incorporated into the magnetite lattice without forming any separate zinc oxide phases. The absence of additional peaks further supports the chemical purity and uniformity of the prepared NPs, reflecting a stable spinel-type structure (Fig S2j)[3, 4].

Table S1 presents the elemental composition of $Zn_xFe_{3-x}O_4$ NPs, confirming the successful incorporation of Zn into the ferrite structure.

Elements	At. No.	Mass (%)	Mass Norm. (%)	Atom (%)	Abs.error (%)
C	6	3.16	3.65	9.96	1.65
O	8	19.96	23.07	47.23	6.99
Fe	26	61.73	71.34	41.84	5.52
Zn	30	1.68	1.94	0.97	0.33
		86.52	**100.00**	**100.00**	

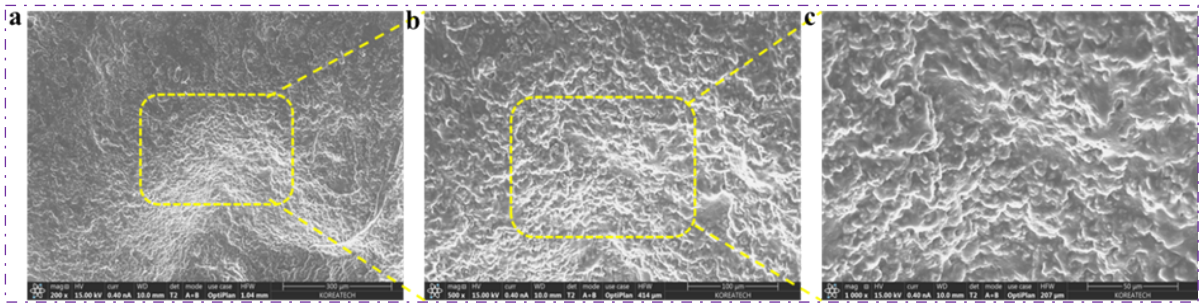

Figure S2. Surface morphology of the $ZnF_{1.50\%}$ n-CH.

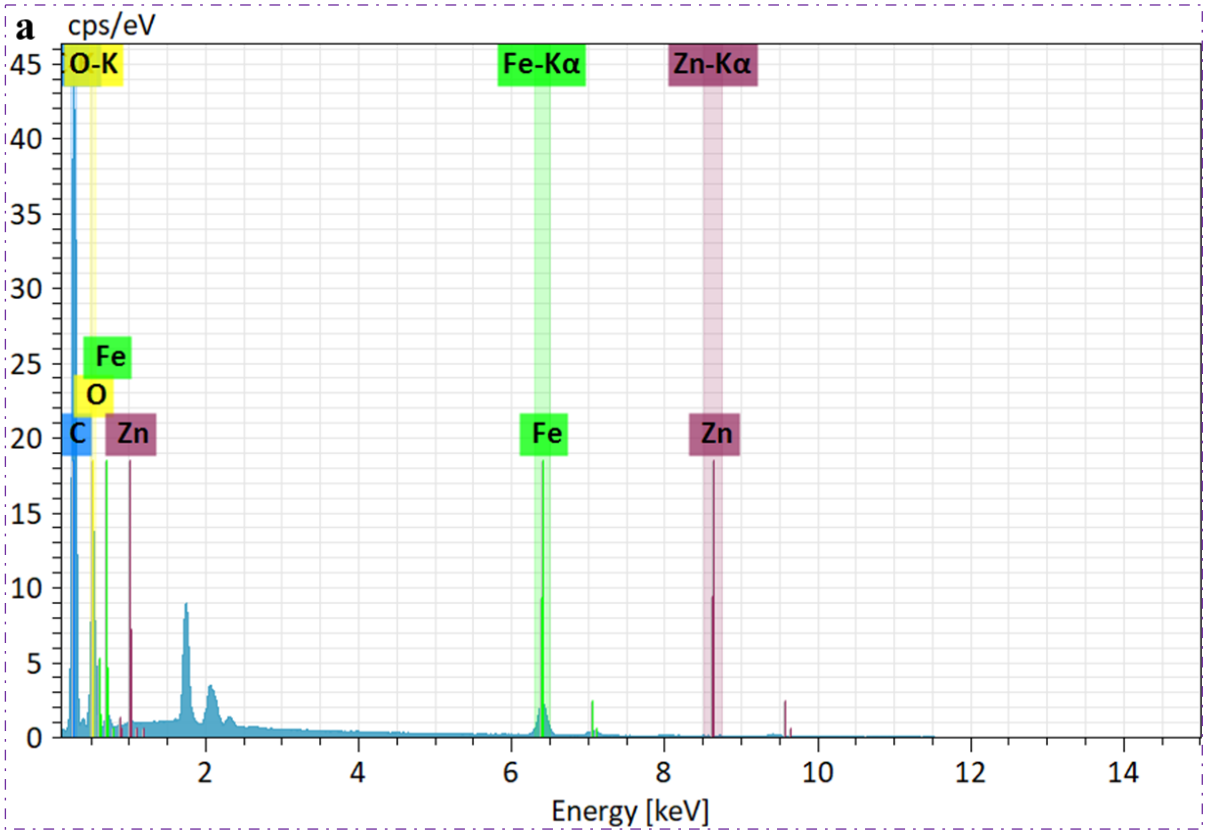

Figure S3 EDS elemental analysis of the $ZnF_{1.00\%}$ n-CH. The spectra and corresponding elemental maps confirm the presence and uniform distribution of Zn, Fe, and O throughout the hydrogel matrix.

Table S2 summarizes the elemental composition of the $ZnF_{1.00\%}$ n-CH determined from EDS analysis.

Elements	At. No.	Mass (%)	Mass Norm. (%)	Atom (%)	Abs.error (%)
C	6	36.30	56.57	68.42	12.00
O	8	20.13	31.37	28.48	7.06
Fe	26	7.21	11.24	2.92	0.73
Zn	30	0.52	0.81	0.18	0.16
		64.16	**100.00**	**100.00**	

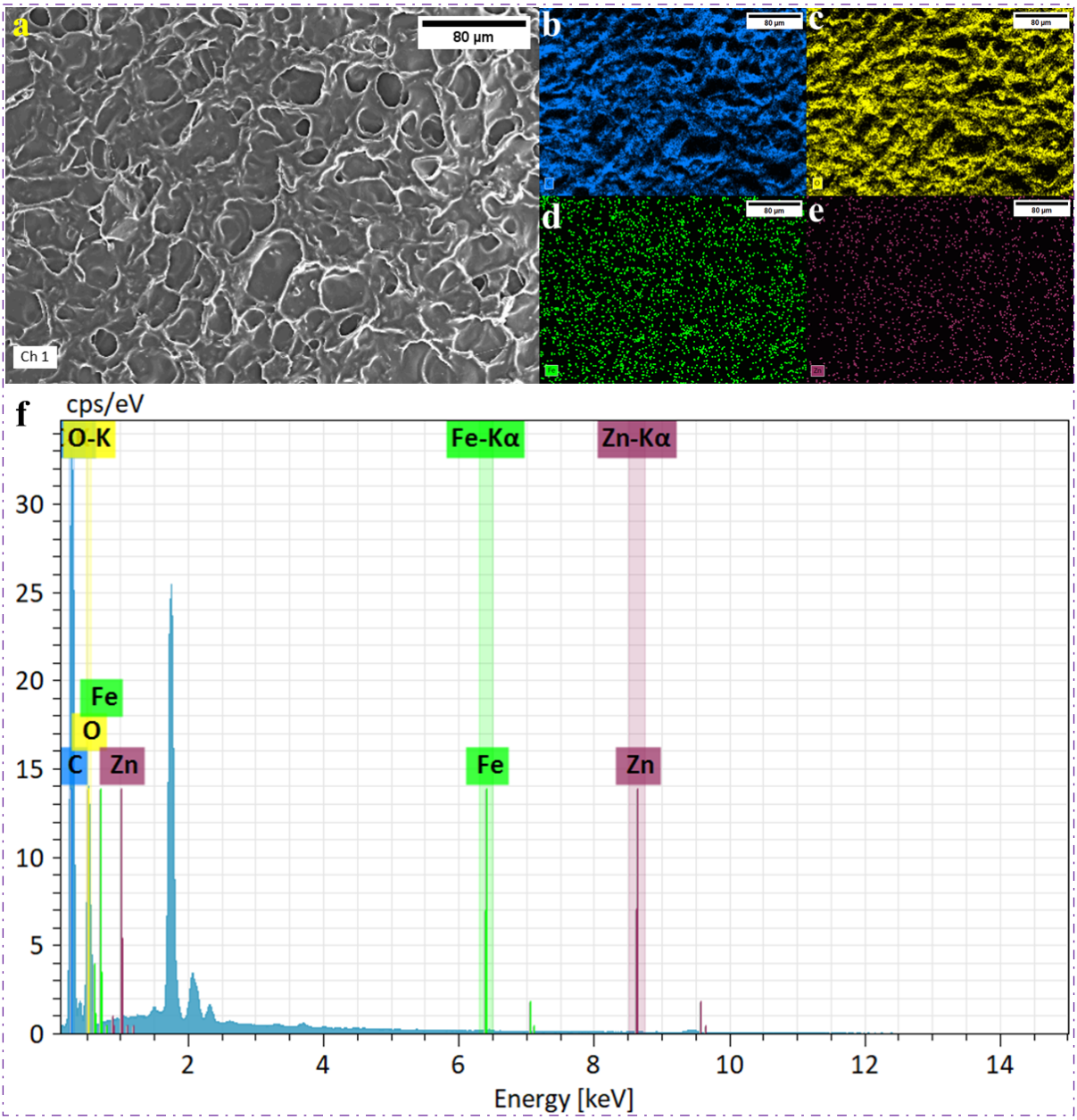

Figure S4. (a-f) Elemental mapping of pristine hydrogel (PH) $ZnF_{0.00\%}$ with respect to Fe, Zn, O and C.

Supporting Information

Table S3 summarizes the elemental composition of the $ZnF_{0.00\%}$ PH determined from EDS analysis.

Elements	At. No.	Mass (%)	Mass Norm. (%)	Atom (%)	Abs.error (%)
C	6	55.70	55.70	62.96	18.62
O	8	43.40	43.40	36.83	15.19
Fe	26	0.59	0.59	0.14	0.16
Zn	30	0.31	0.31	0.07	0.16
		100.0	**100.00**	**100.00**	

Table S4 presents the electrochemical equivalent circuit fitting results for the $ZnF_{x\%}$ n-CHs.

	$ZnF_{0.25\%}$	$ZnF_{0.50\%}$	$ZnF_{1.00\%}$	$ZnF_{1.50\%}$
Elements	Value	Value	Value	Value
Rs	6.42 Ω cm^2	3.051 Ω cm^2	2.463 Ω cm^2	8.854 Ω cm^2
Cdl-T	6.94E-04	2.36E-03	9.89E-04	6.814E-03
Cdl-P	0.56832	0.52868	0.63249	0.5066
Rct	5.481 Ω cm^2	9.669 Ω cm^2	4.225 Ω cm^2	22.42 Ω cm^2
w-T	9.86E-03	7.41E-03	1.15E-02	1.26E-03
w-P	0.501	0.736	0.704	0.842
Chi-Squared	8.74E-06	1.934E-04	3.795E-04	5.8301E-05

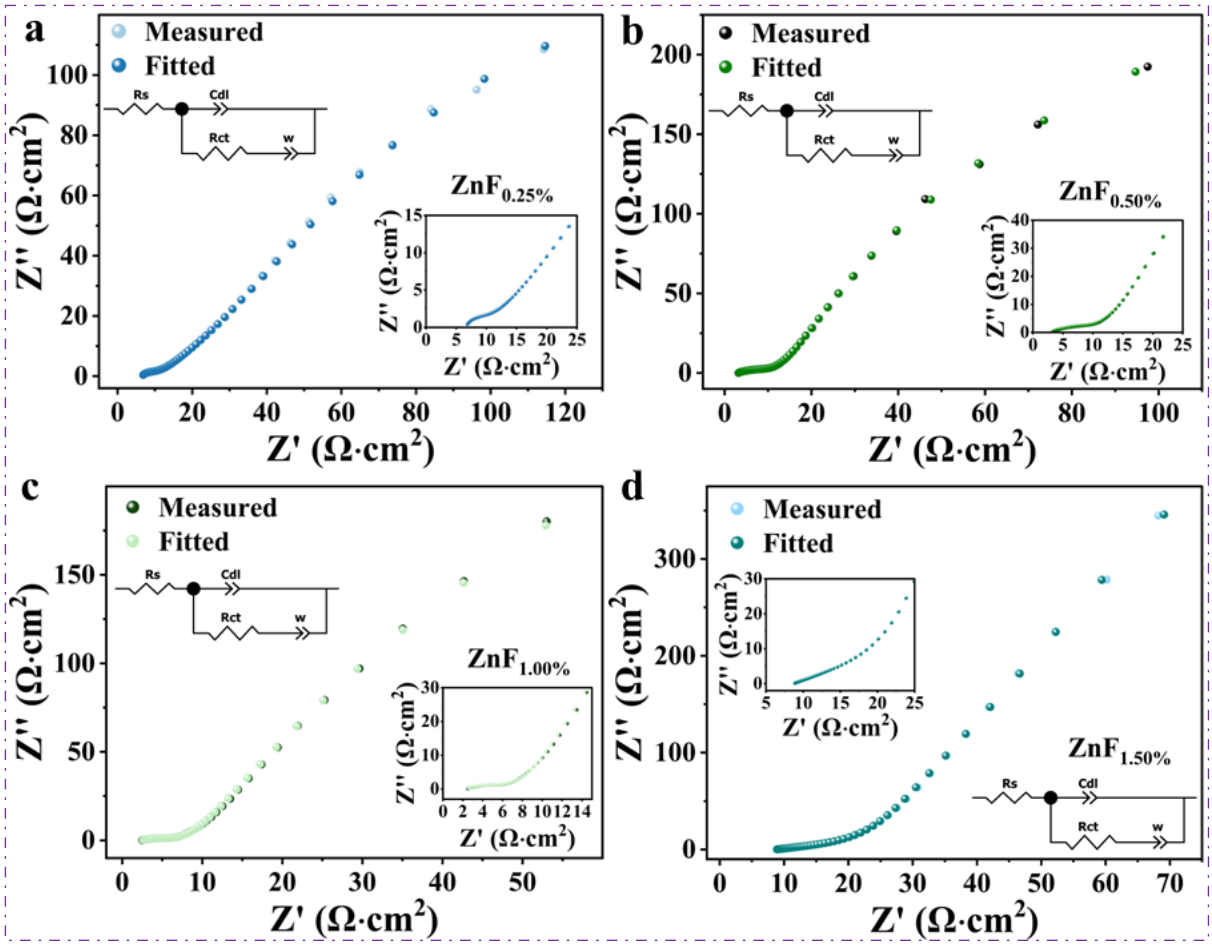

Figure S5. Electrochemical characterization of $ZnF_{x\%}$ n-CHs. **(a–d)** Nyquist plots with equivalent circuit fittings for all compositions.

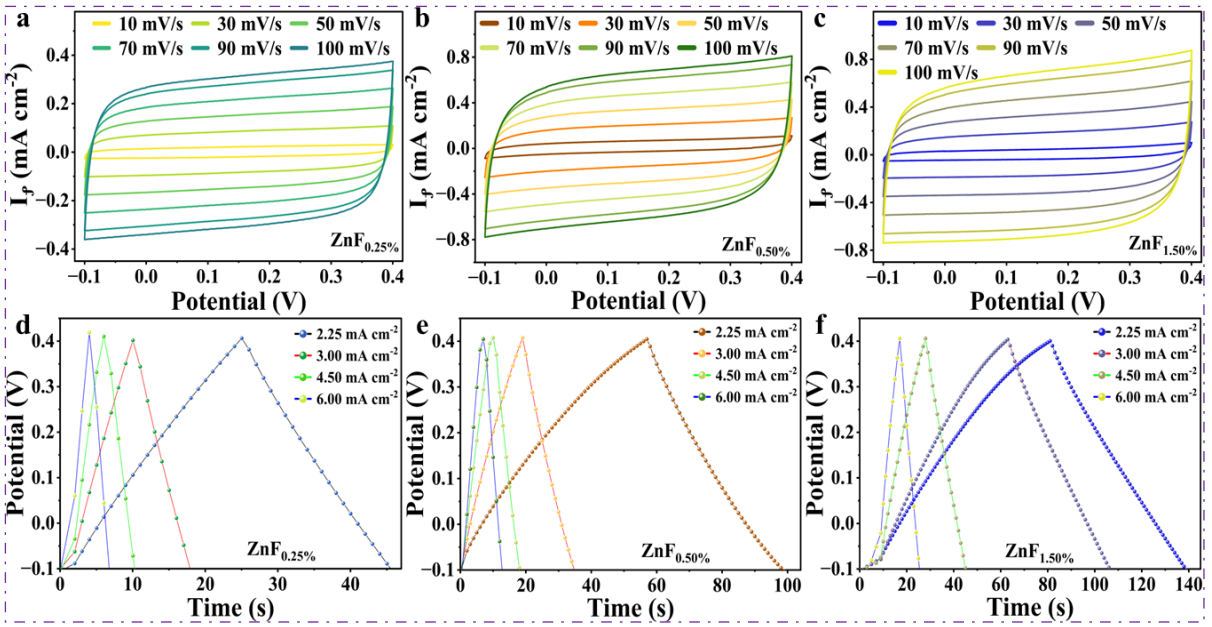

Figure S6. (a–c) CV curves of $ZnF_{x\%}$ n-CHs ($ZnF_{0.25\%, 0.50\% \text{ and } 1.50\%}$) recorded at scan rates of

10 to 100 mV/s, while **(d-f)** GCD profiles of $ZnF_{0.25\%,\ 0.50\%\ and\ 1.50\%}$ at different current densities, respectively.

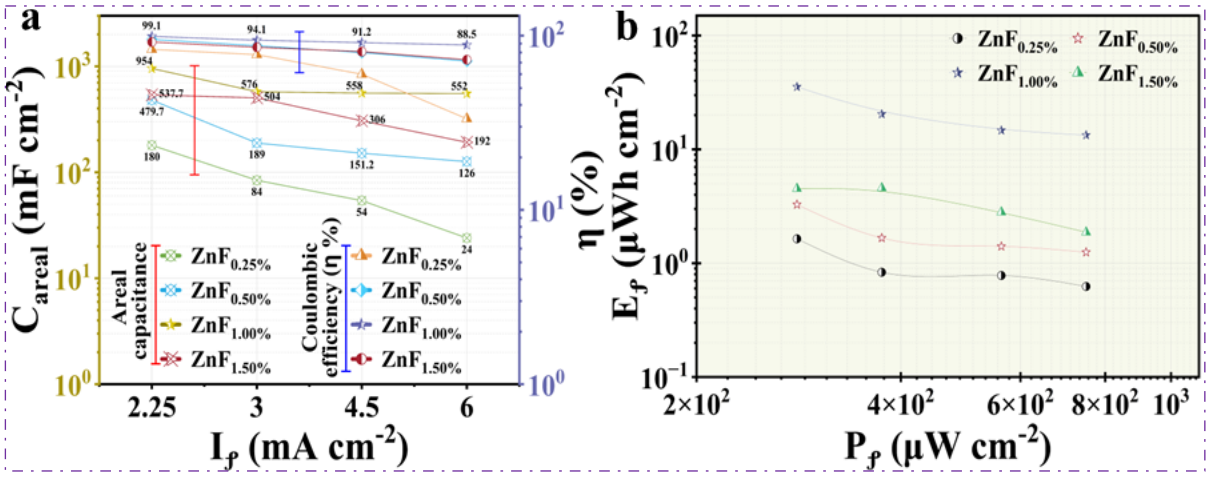

Figure S7. (a) Ragone plot of areal capacitance (C_{areal}) and CE (η%) variation at various current densities of $ZnF_{x\%}$ n-CHs. **(b)** Ragone plot of P_f vs E_f of $ZnF_{x\%}$ n-CH-based SCs.

Table S5 Comparison of areal capacitance, energy density and power density of current work with previously reported composite SCs.

Supporting Information

SC-Materials	Areal Capacitance mF cm^{-1}	Energy density µWh cm^{-2}	Power density µW cm^{-2}	Ref's
PANI/PVA/H2SO4	504	35	100	[45]
poly(2-acrylamido-2-methylpropane sulfonic acid (PAMPS)/PAM-LiCl/EG-PCSCs	202.2	17.9	100	[14]
LIG-MWCNTs	51.975	6.5	219	[36]
ACFM-850/TS carboxymethyl cellulose/NaClO4 composite	888	9.2	130	[50]
p(3, 4-ethylenedioxythiophene)-poly (vinyl alcohol)/poly (ethylene glycol diacrylate), PEDOT-PVA/PEGDA	54.5	4.7	260	[37]
$Mo_2C/MoO_3/PVA/H_2SO_4$	-	42.93	520	[26]
VO2/Au	18	0.45	70	[16]
$Zn@Fe_3O_4$/p(AAm-co-LMA)/IGEPAL®CA-630	954	36	281.3	**Current work**
Device: $ZnF_{1.00\%}$	525.4	146	2625	*

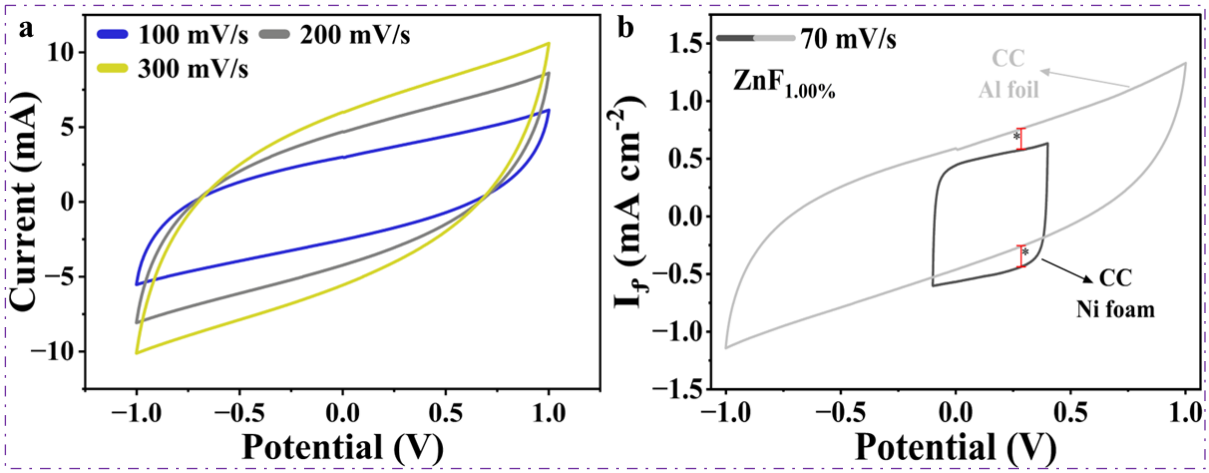

Figure S8. (a) CV curves at different scan rates (100–300 mV s^{-1}) displaying typical EDLC behavior for soft packed supercapacitor $ZnF_{1.00\%}$. **(b)** CV profile of $ZnF_{1.00\%}$ at 70 mV/s showing the area normalization (I_f [mA cm^{-2}]) w.r.t different current collectors (CC).

References

1. Soltanpour, P., R. Naderali, and K. Mabhouti, *Comparative study on structural, morphological, and optical properties of MS/Fe3O4 nanocomposites and M-doped Fe3O4 nanopowders (M= Mn, Zn).* Scientific Reports, 2024. **14**(1): p. 21287.
2. Hayat, A., et al., *Potent antimicrobial and antibiofilm activity of citric acid coated magnetite nanoparticles for leather preservation.* Scientific Reports, 2025. **15**(1): p. 27889.
3. Geng, J., et al., *Preparation of rGO@ Fe 3 O 4 nanocomposite and its application to enhance the thermal conductivity of epoxy resin.* RSC advances, 2021. **11**(27): p. 16592-16599.
4. Qin, H., et al., *A multi-responsive healable supercapacitor.* Nature Communications, 2021. **12**(1): p. 4297.